Int J Clin Exp Med 2026;19(2):66-76
www.ijcem.com /ISSN:1940-5901/IJCEM0163860

Original Article

The study of three-dimensional electroanatomical imaging fusion with cardiac computed tomography (CT) imaging techniques

Pang-Ling Pin[1*], Yan Yang[2*], Zi-Ce Su[2*], Yan-Qing Gong[2], Hao Liu[2], Hong-Zhe Zhang[2], Shi-An Huang[1]

[1]Department of Cardiology, Affiliated Hospital of Guangdong Medical University, Zhanjiang, Guangdong, China; [2]Department of Cardiology, The Seventh Affiliated Hospital of Southern Medical University, Foshan, Guangdong, China. [*]Equal contributors.

Received February 11, 2025; Accepted December 22, 2025; Epub February 15, 2026; Published February 28, 2026

Abstract: Objectives: While the fusion of three-dimensional (3D) cardiac electroanatomical imaging with computed tomography (CT) is a promising approach for guiding radiofrequency ablation (RFA) of arrhythmias, the optimal fusion technique remains undetermined. This study was designed to systematically evaluate and compare the accuracy of prevailing fusion methods to establish an evidence-based standard for clinical practice. Methods: In this prospective study, 30 patients with atrial fibrillation scheduled for ablation were enrolled. All patients underwent pre-operative left atrial CT angiography. Participants were assigned to one of six groups based on the image fusion technique employed: Body Surface, Right Atrial, Aortic, or their respective combinations. Cardiac models were reconstructed from CT data using the CARTO3 system. Image registration was performed by aligning catheter-acquired surface points with the corresponding CT model points. The primary endpoint for assessing accuracy was the mean distance between corresponding landmarks on the CT model and the real-time electroanatomic map. Data are presented as mean ± SD and compared using t-tests or chi-square tests as appropriate. Results: Quantitative analysis revealed significant differences in fusion accuracy among the techniques. The aortic fusion group demonstrated the highest precision with a mean distance of 1.2 ± 0.8 mm, significantly superior to both the body surface group (2.1 ± 1.8 mm) and the right atrial group (3.3 ± 2.2 mm). Conclusions: The aortic fusion method achieves the highest precision for 3D electroanatomical-CT integration in atrial fibrillation ablation procedures. However, considering the balance between procedural complexity, potential vascular risks, and clinical practicality, body surface fusion represents a more viable approach for broader clinical implementation, pending further technical refinements to enhance its accuracy.

Keywords: Three-dimensional (3D) cardiac electroanatomical imaging, electroanatomic mapping, cardiac computed tomography (CT) imaging, image fusion, aortic fusion, radiofrequency ablation, CARTO3 system

Introduction

The growing adoption of radiofrequency ablation (RFA) for arrhythmias has heightened the demand for advanced cardiac imaging guidance [1]. Three-dimensional (3D) electroanatomic mapping systems meet this need by utilizing magnetic or electric fields for real-time catheter navigation [2]. Their core principle involves reconstructing cardiac chamber geometry through extensive endocardial point sampling and superimposing critical electrophysiological data - such as activation time, voltage (for scar identification), and fractionated potentials - onto the anatomical model, thereby generating a comprehensive electroanatomic map [3-6]. This technology is indispensable for guiding catheter ablation of complex arrhythmias, including atrial fibrillation, atrial flutter, and scar-related ventricular tachycardia, and has significantly improved procedural success rates [3, 4, 7]. However, a fundamental limitation of these systems is their suboptimal anatomical accuracy. The reconstructed geometry often exhibits distortions and may not faithfully represent true cardiac anatomy due to constraints such as limited point sampling and catheter instability [8]. To bridge this critical gap between

Table 1. General information of patients

Characteristic	Value/Number (%)
Total patients, n	30
Gender, female/male	13/17
Age, years	65.8 ± 19.3
Type of Atrial Fibrillation	
Paroxysmal	15 (50.0%)
Persistent	9 (30.0%)
Long-standing persistent	6 (20.0%)
Risk Factors	
Hypertension	15 (50.0%)
Smoking	11 (36.7%)
Coronary heart disease	11 (36.7%)
Hyperuricemia	10 (33.3%)
Hyperlipidemia	9 (30.0%)
Heart failure	8 (26.7%)
Alcohol consumption	8 (26.7%)
Diabetes	7 (23.3%)
Obesity	6 (20.0%)

exquisite electrical detail and anatomical imprecision, the integration of electroanatomic maps with pre-acquired computed tomography (CT) images has been developed as a promising solution [9, 10]. Our preliminary research confirms that this fusion approach enhances procedural guidance, enabling complex steps like transseptal puncture with minimal fluoroscopy [11]. While accurate image fusion is paramount, the relative performance of the predominant fusion techniques remains inadequately investigated. A systematic comparison is lacking. Therefore, this study aimed to systematically evaluate and compare the accuracy of three primary fusion techniques - Body Surface, Right Atrial, and Aortic Fusion, along with their combinations - to identify the optimal method for integrating 3D electroanatomic maps with CT images during atrial fibrillation ablation procedures.

Subjects and methods

Subjects

Inclusion Criteria (Patients were enrolled in this study if they met all of the following criteria): (1) Diagnosis of symptomatic, drug-refractory paroxysmal atrial fibrillation (PAF). (2) Scheduled for radiofrequency catheter ablation at the Arrhythmia Specialty Department of Guangdong Medical University Affiliated Hospital between January 2022 and December 2023. (3) Provided written informed consent.

Exclusion Criteria (Patients were excluded from the study if they met any of the following criteria): (1) Known iodine allergy or contraindication to computed tomography angiography (CTA). (2) Pathologies detected on pre-procedural left atrial CTA that increased procedural risk, including: Significant left main trunk coronary artery lesions, Aortic dissection or aortic ulcers, Intracardiac thrombus. (3) General contraindications to radiofrequency ablation surgery (e.g., active infection, uncontrolled heart failure, severe coagulation disorders). (4) Inability or refusal to provide informed consent.

General information is detailed in **Table 1**.

Research methodology

All patients underwent a preoperative left atrial CTA examination. Based on different fusion methods, they were categorized into the following groups: Body Surface Fusion, Right Atrial Fusion, Aortic Fusion, Body Surface-Right Atrial Fusion, Body Surface-Aortic Fusion, and Right Atrial-Aortic Fusion.

The image registration was performed using the CARTO3 system's Registration module [12, 13]. After importing the segmented CT model into the mapping graph, the following steps were undertaken:

(1) Point acquisition: With the patient under stable anesthesia, the ablation catheter was maneuvered to physically touch distinct anatomical landmarks on the patient's chest wall (body surface). These points were acquired in the real-time electroanatomic map [12, 14-16].

(2) Point pairing: Each acquired body surface point was manually and precisely paired with its corresponding landmark on the segmented CT model within the Registration software interface [14, 15].

(3) Registration execution: The software's algorithm (a point-based registration algorithm) was then executed. This algorithm calculated the optimal spatial transformation (including translation and rotation) that would minimize the distance between the set of real-time catheter points and the corresponding set of CT model points.

(4) Fusion and application: Once the optimal transformation was computed and applied, the

Figure 1. Prior to CT scanning, 3 mm steel beads were placed and marked on the manubrium of the sternum and at the mid-axillary line of the fifth intercostal space on the left side.

real-time electroanatomic coordinate system was aligned with the pre-acquired CT coordinate system. This successfully fused the two datasets, allowing the precise display of the catheter's real-time position on the high-resolution CT model.

Left atrial CTA examination and body surface anatomical landmarking method

Unlike the conventional method of left atrial CTA examination [17], in this study, the patients were positioned in the surgical position during the examination, with both hands naturally laid flat without being raised above the head. Instead of taking a deep breath and holding it, the patients were instructed to exhale and then hold their breath while electrocardiogram-gated acquisition of the left atrial CT data was performed. Before undergoing the left atrial CTA, the manubrium of the sternum was divided into three segments, and a marking point was placed at the midpoint of the manubrium, at the upper end of the manubrium at the sternal angle, and at the lower segment of the manubrium just above the xiphoid process. Another marking point was placed at the fifth intercostal space along the mid-axillary line, as shown in **Figure 1**. A spherical steel bead with a diameter of 3 millimeters was then affixed to the marking points with adhesive tape. After completing the left atrial CTA, the steel beads were removed, and the marking points were preserved (**Figure 1**).

CT image sectioning and extraction

Initiate the CARTO3 system and enter the Image Integration interface. Import the DICOM-formatted left atrial CT images into the CARTO3 system. Use the Segmentation software to segment the surface steel beads and various cardiac structures, including the superior vena cava (SVC), right atrium (RA), tricuspid annulus, coronary sinus (CS), right ventricle (RV), pulmonary artery (PA), left atrium (LA), mitral annulus, left ventricle (LV), ascending aorta (AA), left main trunk, and descending aorta. Export the CT images of these anatomical structures to the CARTO mapping graph.

Surface fusion method

Before the surgery begins, expose the chest skin and place a sterile transparent plastic sheet on the patient's chest. Using an ablation catheter (manufactured by Johnson & Johnson), take points at the surface marking points. Utilize the Registration software to fuse the surface points obtained by the ablation catheter with the CT surface points. After fusion, import the SVC, RA, tricuspid annulus, CS, RV, PA, LA, mitral annulus, LV, AA, left main trunk, and descending aorta into the CARTO mapping graph (**Figure 2**).

Right atrial fusion method

Utilize the PANTRAY catheter to thoroughly map the superior vena cava (SVC), right atrium (RA), right atrial appendage, and tricuspid valve. Advance the ablation catheter into the RA to further delineate the coronary sinus (CS), taking a marking point at the ostium of the CS. At the 3 o'clock, 6 o'clock, 9 o'clock, and 12 o'clock positions on the tricuspid annulus, take four marking points. Additionally, take five marking points within and at the mouth of the CS, with the pressure applied by the ablation catheter set at 5 grams. Corresponding matching marking points are taken on the CT model at the respective positions of the SVC, posterior wall of the RA, tricuspid annulus, and CS. Fuse the marking points on the three-dimensional electroanatomic model of the RA with the matching marking points on the CT model (**Figure 3**).

Aortic fusion method

Advance the PANTRAY catheter to the aortic root, aortic arch, and descending aorta for

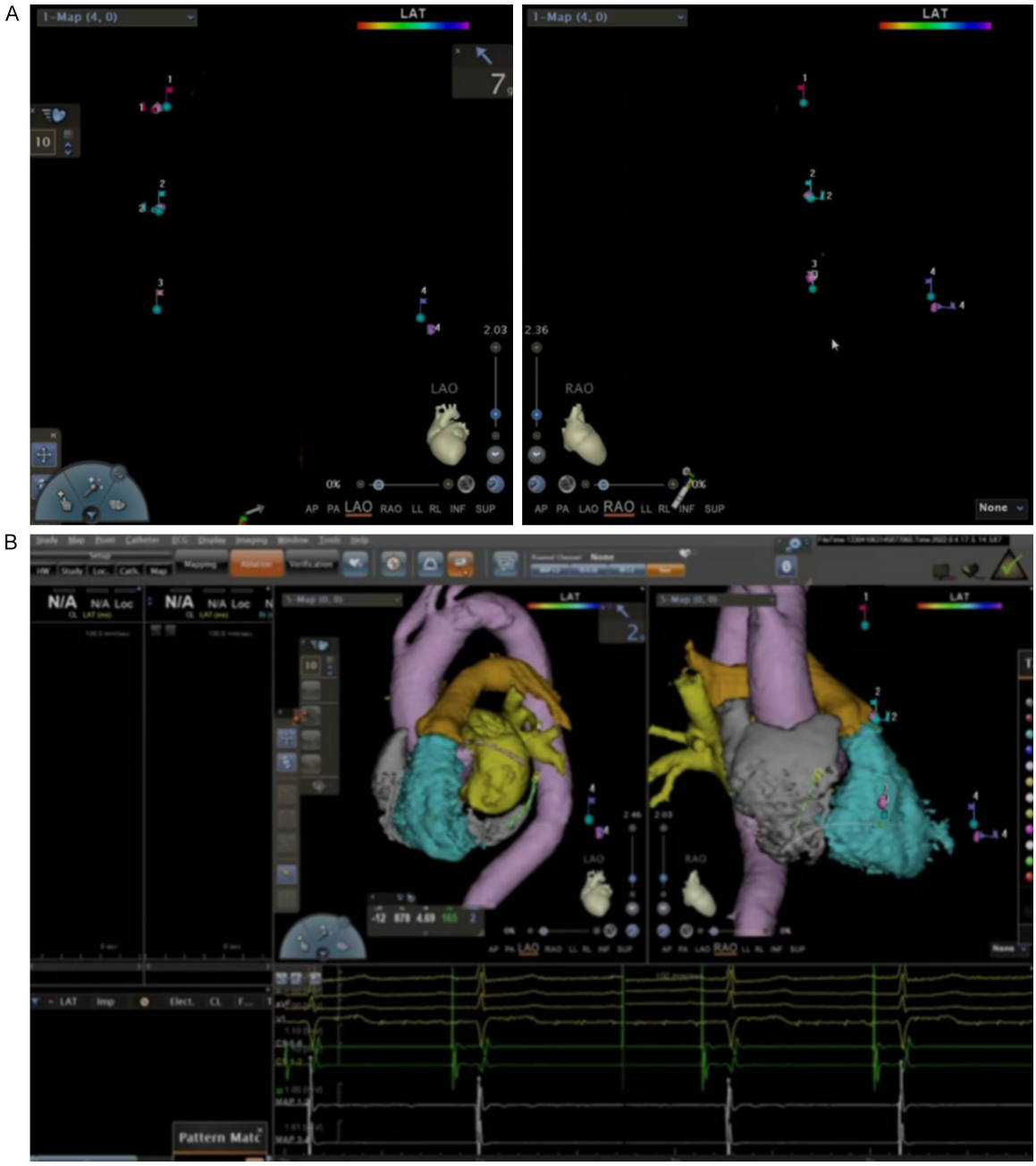

Figure 2. A: Preoperatively, the ablation catheter is used to take points at the steel bead marking points and to fuse these with the steel bead points from the CT images. B: After surface fusion, the anatomical structures of the heart from the CT are imported, using these as a guide for catheter manipulation.

comprehensive mapping. Guide the ablation catheter to the left coronary sinus at the aortic root, identify the ostium of the left main trunk, and take a marking point at this location. Additionally, take marking points in the ascending aorta, the lower edge of the aortic arch, and the descending aorta, maintaining the pressure applied by the ablation catheter at 5 grams. On the CT model, take 10 matching marking points at the left main trunk, ascending aorta, lower edge of the aortic arch, and descending aorta, corresponding to these locations. Fuse the 10 marking points on the three-dimensional electroanatomic model of the left main trunk and aorta with the matching marking points on the CT model (**Figure 4**).

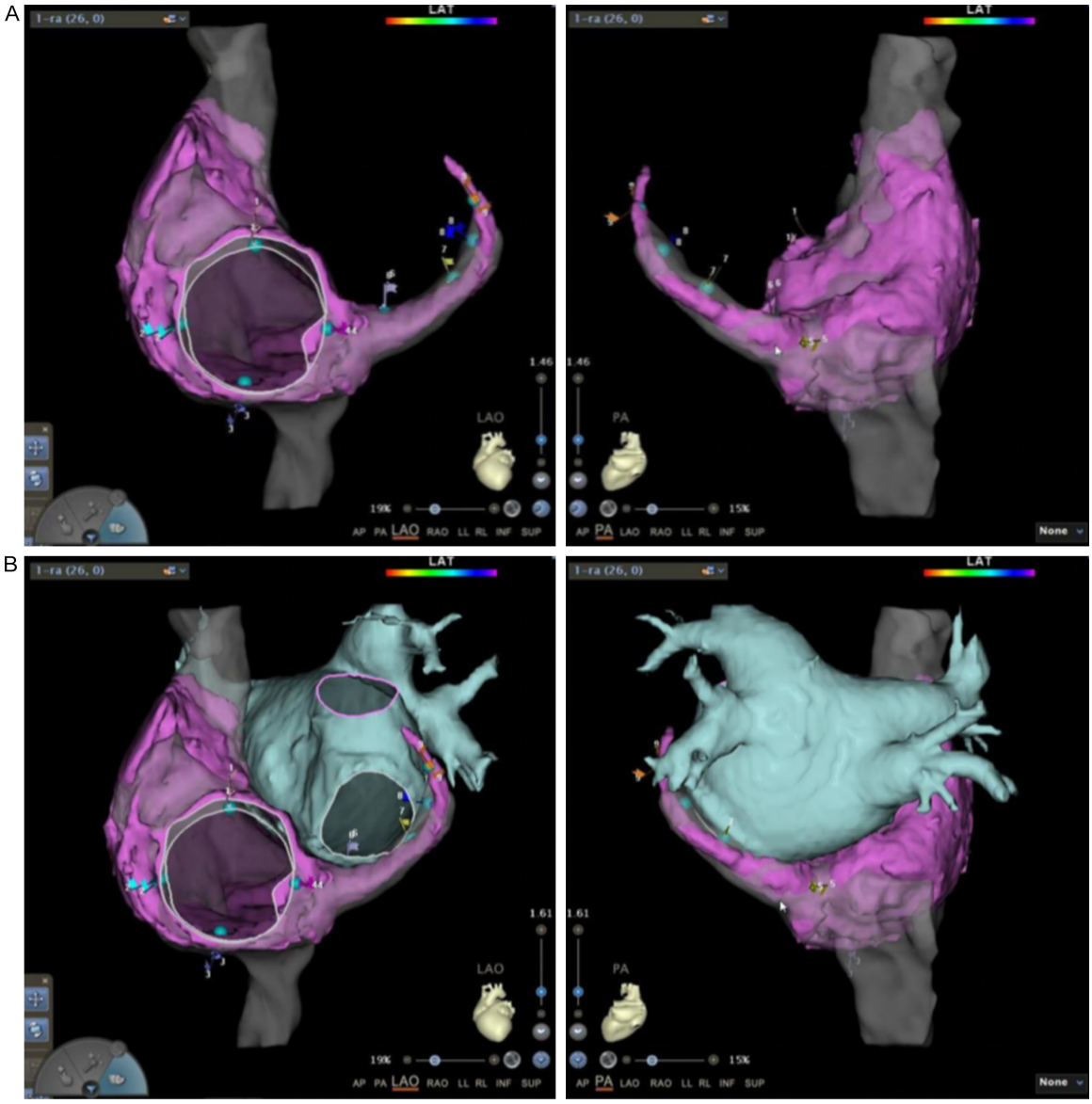

Figure 3. A: Multi-point fusion of the right atrium and coronary sinus. B: After multi-point fusion of the right atrium and coronary sinus, the left atrium is imported.

Verification method for CT fusion effectiveness

Utilize the ablation catheter to take marking points on the left atrial CT model at the anterior and posterior orifices of the left and right pulmonary veins, the top of the left atrium, and the anterior and posterior walls. Introduce an intracardiac ultrasound catheter into the right or left atrium, and use the ultrasound sector scan to visualize each marking point on the CT model. The ultrasound image can display the marking points on the CT model. Corresponding marking points are taken on the endocardial surface of the left atrium using ultrasound. Measure the distance between the CT marking points and the ultrasound marking points on the CT model (**Figure 5**).

Grouping and measurement

Based on the different fusion methods, the subjects are divided into six groups: the Body Surface Fusion group, the Right Atrial Fusion group, and the Aortic Fusion group. For each fusion method, the distance between the marking points on the CT model and the corresponding marking points on the ultrasound at the same location is measured.

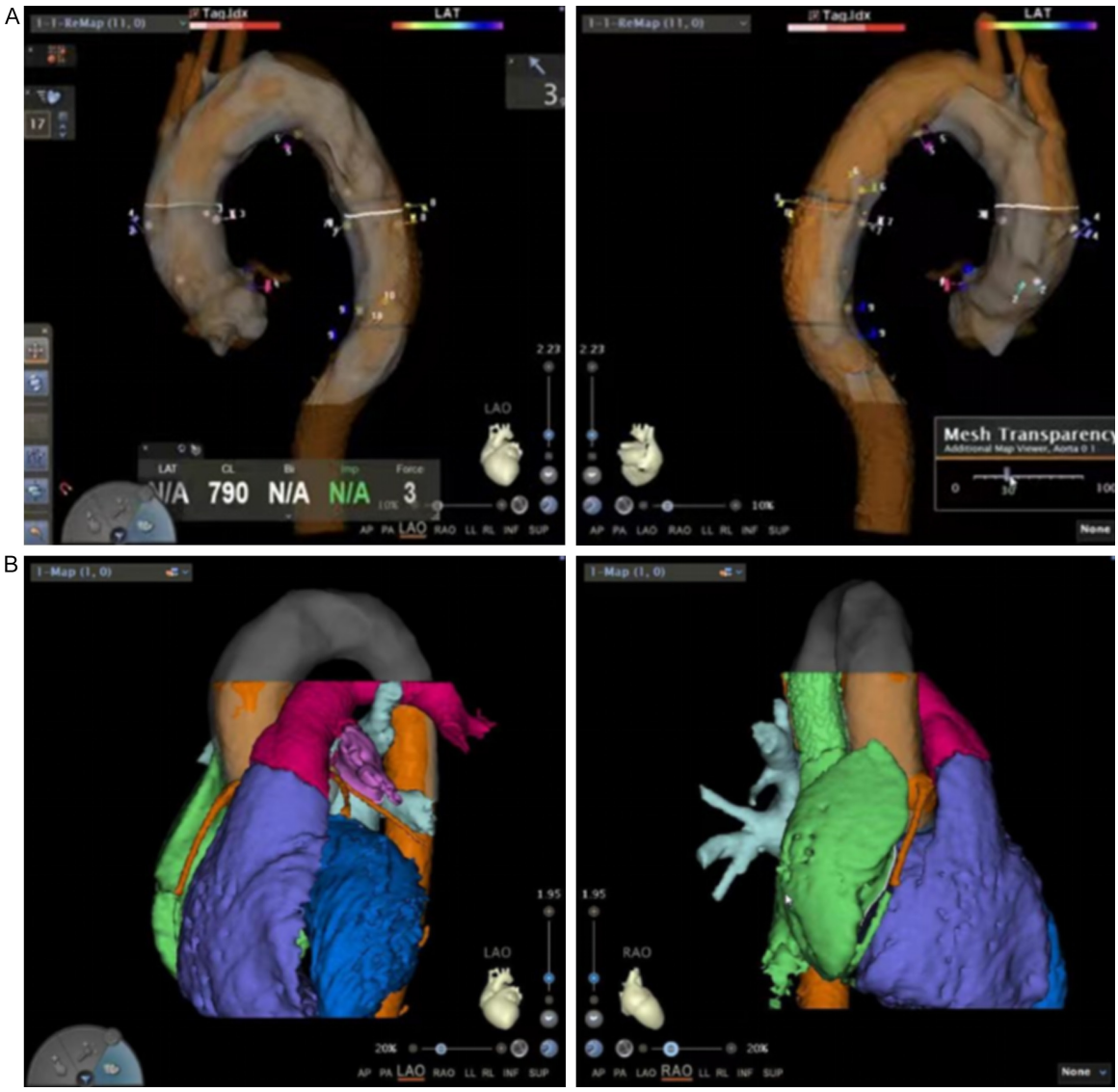

Figure 4. A: The left main trunk is first marked and undergoes single-point fusion, followed by marking points in the ascending aorta, aortic arch, and descending aorta to perform a secondary fusion for calibration. B: The cardiac CT anatomical structures that are imported after the aortic fusion process.

Statistical methods

Quantitative data are expressed as mean ± standard deviation (χ ± s) and analyzed using the t-test or paired t-test as appropriate. Comparisons of rates are performed using the chi-square test.

Results

General information and clinical characteristics of the study population

A total of 30 patients were enrolled in this study. The cohort comprised 17 males (56.7%) and 13 females (43.3%), with a mean age of 65.8 ± 19.3 years. The distribution of atrial fibrillation types was as follows: paroxysmal atrial fibrillation (15 patients, 50%), persistent atrial fibrillation (9 patients, 30%), and long-standing persistent atrial fibrillation (6 patients, 20%).

Regarding cardiovascular risk factors and comorbidities, hypertension was the most prevalent (15 patients, 50%), followed by smoking (11 patients, 36.7%), coronary heart disease (11 patients, 36.7%), and hyperuricemia (10 patients, 33.3%). Other documented condi-

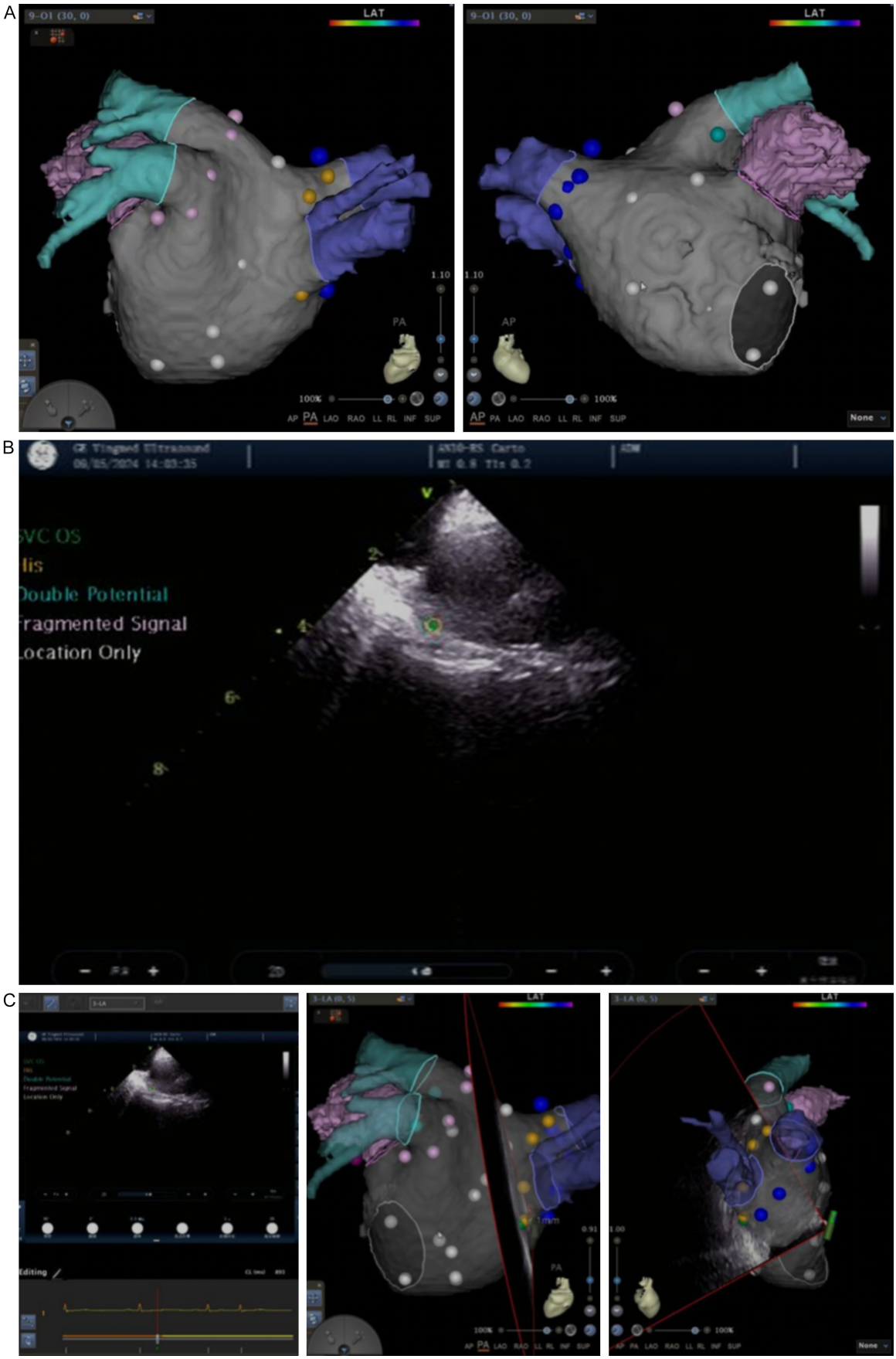
A
LAT
PA
AP
B
Double Potential
Fragmented Signal
Location Only
C
LAT

Figure 5. A: Marking points taken by the ablation catheter on the left atrial CT model at the pulmonary vein ostia, the top, the bottom, the anterior wall, and the posterior wall of the left atrium. B: The yellow circle represents the echocardiographic display of the marking point on the CT model at the posterior wall of the right lower pulmonary vein ostium as visualized on ICE (Intracardiac Echocardiography), while the green marker indicates the corresponding marking point on the endocardial surface of the left atrium as identified by ultrasound. The two points are nearly superimposed. C: Measurement of the distance between the CT marking point and the ultrasound marking point at the same location.

tions included hyperlipidemia (9 patients, 30%), heart failure (8 patients, 26.7%), alcohol consumption (8 patients, 26.7%), diabetes (7 patients, 23.3%), and obesity (6 patients, 20%).

Comparative analysis of fusion accuracy across different techniques

The accuracy of three image fusion techniques was quantitatively assessed by measuring the mean distance between corresponding fiducial points on the fused electroanatomic and CT models. The results demonstrated significant differences in performance among the techniques.

The aortic fusion method achieved the highest precision, with a mean registration error of 1.2 ± 0.8 mm. In contrast, the body surface fusion method yielded an intermediate error of 2.1 ± 1.8 mm, while the right atrial fusion method showed the lowest accuracy, with an error of 3.3 ± 2.2 mm. These findings indicate that the aortic fusion technique provides superior registration accuracy compared to the body surface and right atrial approaches.

Discussion

Image fusion technology can be effectively utilized in atrial fibrillation radiofrequency ablation and the creation of channels between the right and left atria [18, 19]. The critical requirement for successful image fusion technology is precision; inaccuracies can result in misleading guidance [20]. At present, the fusion of three-dimensional cardiac electroanatomical images with CT images predominantly employs a multi-point fusion method, which involves matching and merging landmarks identified on the three-dimensional electroanatomical model with those on the CT images. The process of selecting these landmarks largely depends on visual estimation [21], which is susceptible to error. In this study, six image fusion methods were utilized: the cutaneous fusion method, the right atrial fusion method, the aortic fusion method, the cutaneous combined with right atrial fusion method, the cutaneous combined with aortic fusion method, and the right atrial combined with aortic fusion method.

Body surface merging is a technique that enhances anatomical landmarks on the body surface, which are accurately depicted in computed tomography (CT) images and correspond to points on the three-dimensional electroanatomical cardiac model. Although theoretically capable of precise merging, our research indicates that the accuracy of body surface merging is inferior to that of aortic merging, possibly due to respiratory influences on thoracic landmarks and the spatial relationship between the body surface and the heart. Despite this, body surface merging images effectively guide the manipulation of mapping and ablation catheters within the cardiac chambers and aorta.

Based on our experience, we attribute the suboptimal performance of right atrial fusion to the inherent anatomical challenges of this chamber. The relatively thin myocardium is susceptible to the formation of pseudocavities during 3D modeling, while the lack of distinctive anatomical landmarks increases the likelihood of visual errors - these observations explain why this method demonstrated the largest registration error in our study. The lack of distinctive anatomical landmarks in the right atrium further increases the likelihood of visual errors during the merging process. The accuracy of right atrial merging depends on the precise selection of points on the electroanatomical model. The tricuspid annulus, with its unique electrophysiological characteristics (A/V ratio close to 1:1), facilitates the identification of landmarks at the 3, 6, 9, and 12 o'clock positions. The confined spatial dimensions of the coronary sinus and the superior and inferior vena cava minimize errors in landmark placement within the coronary sinus. To construct the tricuspid annulus, it is recommended to use a PENTRAY catheter to model the right atrium by advancing in four directions (superior, inferi-

or, medial, and lateral), then erasing the right ventricular portion while preserving the tricuspid valve. The ablation catheter should then identify the tricuspid annulus landmarks based on the A/V ratio. The coronary sinus is constructed using an ablation catheter for modeling, with landmarks acquired during this process. During landmark acquisition, the ablation catheter should maintain a pressure of 5 grams to ensure adequate contact without causing protrusion.

The aortic wall is relatively thick, minimizing the occurrence of false lumens during PENTRAY-assisted modeling and thereby reducing errors associated with aortic fusion. During the extraction of the aortic CT model, the aorta is segmented into the ascending aorta, the aortic arch, and the descending aorta. Comprehensive modeling of the aortic sinuses, ascending aorta, and descending aorta is performed using a PENTRAY catheter before aortic fusion. A mapping or ablation catheter is advanced to the ostium of the left main coronary artery to obtain marked points. Initially, a single-point fusion of the left main coronary artery is executed, followed by calibration using points from the anterior, posterior, medial, and lateral aspects of the cross-sections of the ascending and descending aorta. The entry of the ablation catheter into the ostium of the left main coronary artery is determined by two criteria: 1) the presence of A and V waves on the distal electrode potential of the catheter; and 2) a significant increase in the impedance of the ablation catheter, exceeding an elevation of 50 ohms.

We interpret this finding as a direct consequence of the anatomical stability of the aorta. Unlike the thoracic wall, which is subject to respiratory motion, or the thin-walled right atrium, which is prone to geometric distortion during catheter manipulation, the aortic wall provides a rigid and spatially stable reference structure for image registration, thereby minimizing error propagation. However, elderly patients frequently present with concurrent aortic and left main coronary artery pathologies, introducing certain procedural risks. Additionally, femoral artery puncture may increase the risk of pseudoaneurysm and arteriovenous fistula formation. Aortic fusion may also entail additional procedural steps, prolonging the surgical duration. Consequently, we posit that for many routine clinical scenarios, body surface fusion presents a more favorable risk-benefit profile due to its simplicity and non-invasive nature, reserving aortic fusion for cases where supreme accuracy is paramount. This represents our recommended clinical pathway based on the risk-benefit analysis derived from our findings.

Despite its contributions, this study has several limitations that should be acknowledged. First, the sample size, though sufficient for an initial technical comparison, is relatively modest. We anticipate that future studies with larger, multicenter cohorts will help validate the generalizability of our findings. Second, we recognize that the single-center design may influence the results. Most importantly, we are particularly interested in exploring whether the superior accuracy of aortic fusion translates into measurably improved patient outcomes in a long-term, randomized trial. Looking forward, we expect and encourage future research to concentrate on refining the body surface fusion technique, perhaps through the implementation of advanced respiratory gating algorithms. Furthermore, we envision the development of fully automated, robust fusion algorithms that minimize the subjective component of landmark selection - this represents a key direction for future technological advancement in this field.

Disclosure of conflict of interest

None.

Address correspondence to: Hong-Zhe Zhang, Department of Cardiology, The Seventh Affiliated Hospital, Southern Medical University, Desheng Road Section 28, Foshan 528200, Guangdong, China. Tel: +86-0757-85631264; E-mail: zhz259-3620@smu.edu.cn; Shi-An Huang, Department of Cardiology, Affiliated Hospital of Guangdong Medical College, Zhanjiang 524001, Guangdong, China. Tel: +86-0757-85631264; E-mail: huangshian1969@126.com

References

[1] Matoshvili Z, Bastani H, Bourke T, Braunschweig F, Drca N, Gudmundsson K, Insulander P, Jemtrén A, Kennebäck G, Saluveer O, Schwieler J, Tapanainen J, Wredlert C and Jensen-Urstad M. Safety of fluoroscopy-guided transseptal approach for ablation of left-sided arrhythmias. Europace 2017; 19: 2023-2026.

[2] Narayan SM and John RM. Advanced electroanatomic mapping: current and emerging approaches. Curr Treat Options Cardiovasc Med 2024; 26: 69-91.
[3] Yu R, Liu N, Lu J, Zhao X, Hu Y, Zhang J, Xu F, Tang R, Bai R, Akar JG, Dong J and Ma C. 3-dimensional transseptal puncture based on electrographic characteristics of fossa ovalis: a fluoroscopy-free and echocardiography-free method. JACC Cardiovasc Interv 2020; 13: 1223-1232.
[4] Maury P, Monteil B, Marty L, Duparc A, Mondoly P and Rollin A. Three-dimensional mapping in the electrophysiological laboratory. Arch Cardiovasc Dis 2018; 111: 456-464.
[5] Althoff TF, Anderson RH, Goetz C, Petersen SE, Díaz PM, Nijveldt R, Maurovich-Horvat P, Bax J, Hussain S, Schmidt C, Spicer DE, Sanchez-Quintana D, Corsi C, Dössel O, Climent AM, Rodriguez B, Schotten U, Loewe A, Guillem MS, Cabrera JÁ, Merino JL, Wijnmaalen AP, Bertrand PB, de Groot N, Derval N, Didenko M, Donal E, Dweck MR and Ho SY. Regionalization of the atria for 3D electroanatomical mapping, cardiac imaging, and computational modelling: a clinical consensus statement of the European Heart Rhythm Association and the European Association of Cardiovascular Imaging of the ESC. Europace 2025; 27: euaf134.
[6] Robles AG, Jan M, Prolič Kalinšek T, Antolič B, Rauber M, Klemen L, Šinkovec M, Romano S, Sciarra L and Pernat A. How imaging techniques improve ventricular arrhythmia ablation: a multimodality-based approach. J Clin Med 2023; 12: 7420.
[7] Tops LF, Bax JJ, Zeppenfeld K, Jongbloed MR, Lamb HJ, van der Wall EE and Schalij MJ. Fusion of multislice computed tomography imaging with three-dimensional electroanatomic mapping to guide radiofrequency catheter ablation procedures. Heart Rhythm 2005; 2: 1076-1081.
[8] Bohnen M, Minners J, Eichenlaub M, Weber R, Allgeier HJ, Jadidi A, Neumann FJ, Westermann D, Arentz T and Lehrmann H. Feasibility and safety of a three-dimensional anatomic map-guided transseptal puncture for left-sided catheter ablation procedures. Europace 2023; 25: 1126-1134.
[9] Maragiannis K, Benz DC, Saguner AM, Breitenstein A, Michel J, Pazhenkottil AP, Kaufmann PA, Buechel RR and Giannopoulos AA. Cardiac CT for electrophysiological interventions. Int J Cardiovasc Imaging 2025; 41: 1259-1275.
[10] Zou S, Jia R, Zhou X, Hao Y, Lu S, Guo R, Yang W, Cen Z, Gong S, Li J and Cui K. Merging three-dimensional CT with electroanatomic mapping facilitates ablation of ventricular arrhythmias originating from aortic root and great cardiac vein. J Interv Card Electrophysiol 2021; 60: 101-108.
[11] Baykaner T, Quadros KK, Thosani A, Yasmeh B, Mitra R, Liu E, Belden W, Liu Z, Costea A, Brodt CR and Zei PC. Safety and efficacy of zero fluoroscopy transseptal puncture with different approaches. Pacing Clin Electrophysiol 2020; 43: 12-18.
[12] Zoppo F, Gagno G, Perazza L, Cocciolo A, Mugnai G, Vaccari D and Calzolari V. Electroanatomic voltage mapping and characterisation imaging for "right ventricle arrhythmic syndromes" beyond the arrhythmia definition: a comprehensive review. Int J Cardiovasc Imaging 2021; 37: 2347-2357.
[13] Landra F, Saglietto A, Falasconi G, Penela D, Soto-Iglesias D, Curti E, Tonello B, Teresi L, Turturiello D, Franco-Ocaña P, Gigante C, Valeriano C, Capobianco C, Francia P, Alderete J, Viveros D, Bellido AF, Zaraket F, Martí-Almor J, Cameli M and Berruezo A. Left atrial intramyocardial fat at pulmonary vein reconnection sites during atrial fibrillation redo ablation. Europace 2025; 27: euaf038.
[14] Brett CL, Cook JA, Aboud AA, Karim R, Shinohara ET and Stevenson WG. Novel workflow for conversion of catheter-based electroanatomic mapping to DICOM imaging for noninvasive radioablation of ventricular tachycardia. Pract Radiat Oncol 2021; 11: 84-88.
[15] Rigal L, Benali K, Barré V, Bougault M, Bellec J, Crevoisier R, Martins R and Simon A. Multimodal fusion workflow for target delineation in cardiac radioablation of ventricular tachycardia. Med Phys 2024; 51: 292-305.
[16] Conte E, Carbucicchio C, Catto V, Kochi AN, Mushtaq S, De Iuliis PG, Guglielmo M, Baggiano A, Sattin T, Pontone G, Pepi M, Tondo C and Andreini D. Live integration of comprehensive cardiac CT with electroanatomical mapping in patients with refractory ventricular tachycardia. J Cardiovasc Comput Tomogr 2022; 16: 262-265.
[17] Kern MJ and Seto AH. Transseptal puncture guided by electroanatomic mapping: a novel fluoroscopically and echocardiographically free method. JACC Cardiovasc Interv 2020; 13: 1233-1235.
[18] Jiang C, Liu Q, Chen S, Callans DJ and Ren JF. Fluoroscopy-free transseptal catheterization and atrial fibrillation ablation: intracardiac echocardiography needed. JACC Cardiovasc Interv 2020; 13: 2084-2085.
[19] Ejima K, Shoda M, Yagishita D, Futagawa K, Yashiro B, Sato T, Manaka T, Nakajima T, Ohmori H and Hagiwara N. Image integration of three-dimensional cone-beam computed to-

mography angiogram into electroanatomical mapping system to guide catheter ablation of atrial fibrillation. Europace 2010; 12: 45-51.
[20] Fingrova Z, Marek J, Havranek S, Lambert L, Kuchynka P and Linhart A. 3D electroanatomical mapping is less sensitive to atrial remodeling in estimation of true left atrial volume than echocardiography. BMC Med Imaging 2018; 18: 32.
[21] Hertel JN, Jerltorp K, Hansen MEH, Isaksen JL, Sattler SM, Linz B, Chaldoupi SM, Jespersen T, Saljic A, Gang U, Manninger M and Linz D. 3D-electroanatomical mapping of the left atrium and catheter-based pulmonary vein isolation in pigs: a practical guide. Front Cardiovasc Med 2023; 10: 1139364.